Article

Cell Chemical Biology

Functional Plasticity of the AgrC Receptor Histidine Kinase Required for Staphylococcal Virulence

Graphical Abstract

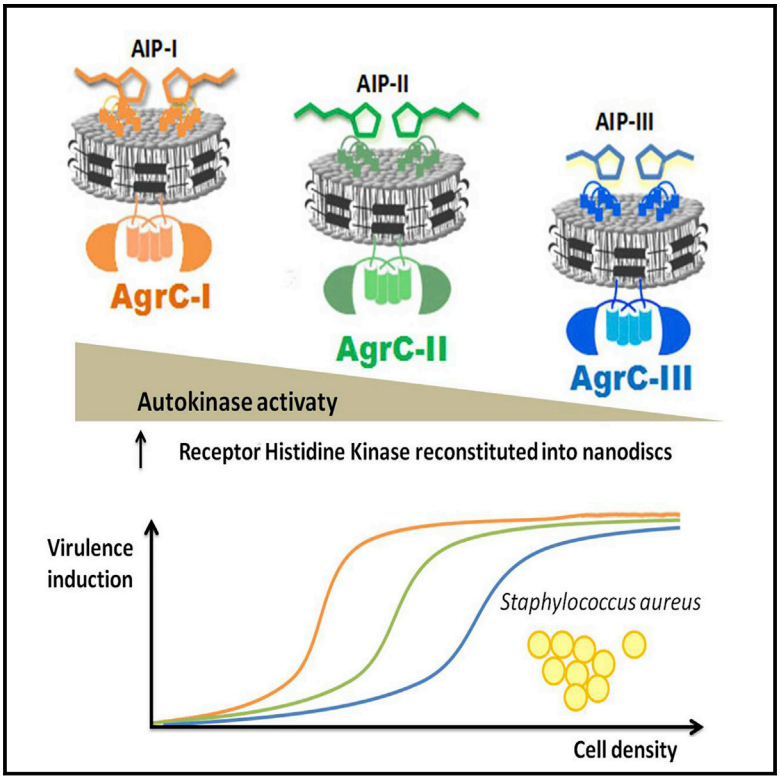

Highlights

- AgrC activity correlates with the timing of *agr* induction among *S. aureus* subgroups
- Single mutations in AgrC produce constitutive mutants by modifying the response curve
- AgrC constitutive mutants differ in phospho-transfer rate with non-cognate AIP bound

Authors

Boyuan Wang, Aishan Zhao, Qian Xie, Paul Dominic Olinares, Brian T. Chait, Richard P. Novick, Tom W. Muir

Correspondence

muir@princeton.edu

In Brief

Sequence variants of AgrC, a receptor histidine kinase involved in virulence regulation in *S. aureus*, show different activity depending on the conformational output of the sensor domain. Single mutations in AgrC generate constitutive mutants through modification of the response curve, and these mutants phosphorylate AgrA at different rates in the presence of inhibitors, revealing a key regulatory hot spot.

Wang et al., 2017, Cell Chemical Biology *24*, 1–11
January 19, 2017
http://dx.doi.org/10.1016/j.chembiol.2016.12.008

CellPress

Please cite this article in press as: Wang et al., Functional Plasticity of the AgrC Receptor Histidine Kinase Required for Staphylococcal Virulence, Cell Chemical Biology (2016), http://dx.doi.org/10.1016/j.chembiol.2016.12.008

Cell Chemical Biology
Article

Functional Plasticity of the AgrC Receptor Histidine Kinase Required for Staphylococcal Virulence

Boyuan Wang,[1,2,5,6] Aishan Zhao,[1,5] Qian Xie,[1] Paul Dominic Olinares,[3] Brian T. Chait,[3] Richard P. Novick,[4] and Tom W. Muir[1,7,*]

[1]Department of Chemistry, Frick Chemistry Laboratory, Princeton University, Washington Road, Princeton, NJ 08544-0015, USA
[2]Graduate Program, The Rockefeller University, 1230 York Avenue, New York, NY 10065, USA
[3]Laboratory of Mass Spectrometry and Gaseous Ion Chemistry, The Rockefeller University, 1230 York Avenue, New York, NY 10065, USA
[4]Department of Microbiology, Skirball Institute, NYU Medical Center, 540-562 First Avenue, New York, NY 10016, USA
[5]Co-first author
[6]Present address: Department of Biology, Massachusetts Institute of Technology, 400 Main Street, Cambridge, MA 02139, USA
[7]Lead Contact
*Correspondence: muir@princeton.edu
http://dx.doi.org/10.1016/j.chembiol.2016.12.008

SUMMARY

Staphylococcus aureus **employs the receptor histidine kinase (RHK), AgrC, to detect quorum-sensing (QS) pheromones, the autoinducer peptides (AIPs), which regulate the virulence of the bacterium. Variation in the QS circuit divides *S. aureus* into four subgroups, each producing a specific AIP-AgrC pair. While the timing of QS induction is known to differ among these subgroups, the molecular basis of this phenomenon is unknown. Here, we report the successful reconstitution of several AgrC variants and show that the agonist-induced activity of the receptors varies in a manner that accounts for these temporal differences in QS induction. Our studies also reveal a key regulatory hotspot on AgrC that controls the basal activity of RHK as well as the responsiveness of the system to ligand inputs. Collectively, these studies offer insights into the capacity of the RHK for adaptive evolution.**

INTRODUCTION

Two-component signaling systems (TCSs) exist in all three domains of life and are harnessed by the host organisms to expeditiously sense and respond to environmental stimuli (Krell et al., 2010). All prototypic TCSs have a receptor histidine kinase (RHK) component that acts as the starting point of a phosphotransfer cascade and a response regulator (RR) that functions as the phosphoryl acceptor. The RHK adopts a modular architecture, containing an HK module that possesses all biochemical activities and one or more sensory modules, or sensors, which regulate the activity of the HK module in response to the cognate stimuli (Gao and Stock, 2009). The conformational state of the sensor(s) is propagated to the HK module and, thereby, dictates the activity state of the RHK (Casino et al., 2010). In this regard, the enzymatic activity of an RHK depends upon two features of the system: (1) the conformational input from the sensor(s) and (2) the correlation between the HK-module activity and the input variable, which we refer to as the input-response relationship. While the former factor has been elucidated for numerous RHKs by structural studies performed on either isolated sensors or full-length receptors (for a recent review see, Bhate et al., 2015), information regarding the latter is relatively scarce. Nonetheless, the input-response relationship of an HK module underlies the likelihood of a functional sensory system emerging from the recombination of HK and sensor domains (Capra and Laub, 2012) and is therefore critical to our understanding of the enormous diversity and prevalence of TCSs.

All HK modules consist of at least two subdomains, namely the DHp (dimerization and histidine phosphorylation) and the CA (catalytic and ATP binding) (Gao and Stock, 2009). The N-terminal DHp subdomain folds into an α-helical hairpin and mediates the homo-dimerization of RHKs through four-helix-bundle formation. The C-terminal CA subdomain binds to the nucleotide triphosphate cofactor and catalyzes the phosphorylation to a histidine residue in the DHp subdomain, a process called autophosphorylation. Most phosphorylated RHKs donate the phosphoryl group to, and thereby switch the activity state of, their cognate RR. Some HK modules may also act as phosphatases to their cognate RRs, an activity also dependent upon the DHp conformation (Gao and Stock, 2009). Typically, the DHp subdomain is located next to the sensory module in the primary sequence and is therefore directly influenced by the conformational input. Accordingly, structural rearrangements of the DHp four-helix bundle have been shown to switch the HK module between kinase-off and -on states by displaying different surfaces for the docking of the CA subdomain (Figure 1A) (Marina et al., 2005; Mechaly et al., 2014; Wang et al., 2013). One approach for studying the input-response relationship of an HK module is to make systematic perturbations to the DHp conformational state. This has been accomplished employing protein-chimera approaches in which judicious placement of a heterologous fusion element controls the orientation of the N-terminal helices in the DHp dimer (Moglich et al., 2009; Wang et al., 2014). Using such a chimera strategy (Figures 1B–1E, see Results for details), we have recently shown that the HK activity of *Staphylococcus aureus* AgrC changes gradually with the magnitude of twisting motions (Wang et al., 2014).

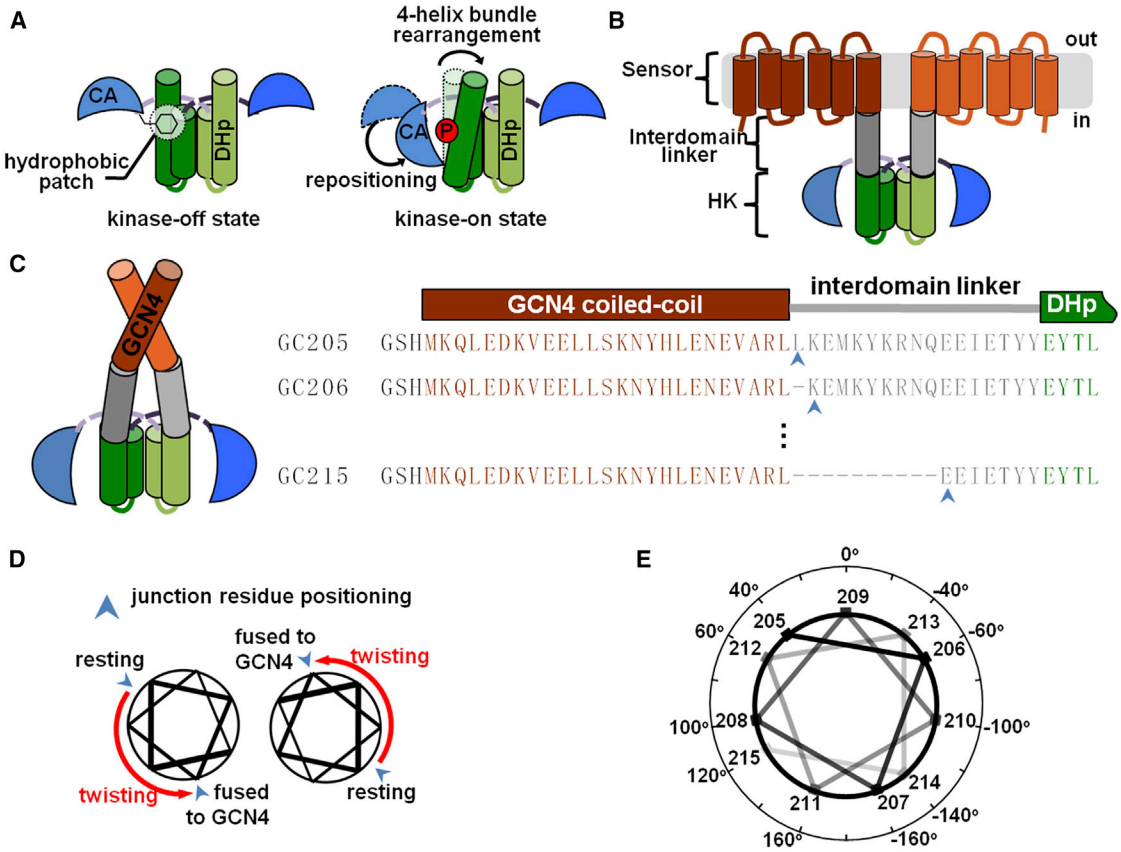

Figure 1. GCN4-AgrC Chimera Approach to Manipulate the Conformation of an AgrC HK Module

(A) Model for the autokinase activation in an HK module: in the kinase-off state (left panel), the CA subdomain (blue) docks on a hydrophobic patch on the DHp four-helix bundle. Structural rearrangement that sequesters this hydrophobic patch activates the HK by allowing the CA to re-position at the phospho-acceptor histidine.

(B) Domain architecture of AgrC-I. The protein is shown as a homodimer with the sensor module and DHp and CA subdomains colored in brown, green, and blue, respectively. The helical interdomain linkers are highlighted as gray cylinders.

(C and D) Design principles of GCN4-AgrC chimera proteins. Diagrams show the sequences around the fusion junction (C) and the presumed twisting of the register of the AgrC residues (indicated by blue arrowheads) at the junction as a consequence of fusion to the GCN4 coiled coil (D).

(E) Calculation of the register deviation of AgrC residues 205–215 from residue 209. Numbers outside the outer circle indicate the putative magnitude of the twisting movement imposed on the interdomain linker pair after fusing the corresponding position (marked inside the outer circle) to GCN4.

AgrC contains a membrane-integrated sensor and an HK module flanking a short interdomain linker. In *S. aureus*, this RHK is one of four Agr proteins that constitute the quorum-sensing (QS) machinery (Figure S1). All Agr proteins are encoded by the same operon in the pleiotropic *agr* locus, the deletion of which causes a severe defect in virulence and survival of the bacterium in mammalian hosts (Ji et al., 1997; Novick and Geisinger, 2008; Wang and Muir, 2016). Specifically, AgrB and AgrD are involved in the production of the autoinducer peptide (AIP) (Figure S1), which acts as a proxy of the population density (Qiu et al., 2005; Wang et al., 2015). AgrC detects AIP, and is therefore activated when the bacterial population reaches a threshold density (Lyon et al., 2002a; Wang et al., 2014). Phospho-transfer from AgrC activates AgrA, an RR and transcription factor that upregulates the transcription of *agr* genes when bound to promoter element P2 and regulates virulence protein production when bound to promotor P3 (Koenig et al., 2004). Four subgroups of *S. aureus* have been identified from clinical isolates, each featuring a variant of the *agr* allele producing a unique, activating AIP-AgrC pair (Jarraud et al., 2000; Ji et al., 1997). Each subgroup holds its identity at the molecular level, as heterologous AIP-AgrC interactions are in general inhibitory. Intriguingly, induction of the AgrC-AgrA TCS does not occur at an identical population density in all subgroups: groups I and IV confer the earliest induction and group III the latest (Geisinger et al., 2012). Conceivably, such phenotypic differences foreshadow divergence among AgrC variants regarding their biochemical activities, although this idea is yet to be experimentally tested. Aside from the native variants of AgrC, our previous studies have identified several constitutively active mutants of AgrC from group I *S. aureus* cells (AgrC-I), i.e., those capable of turning on the QS signaling independent of the cognate AIP-I. Mutations conferring the most robust constitutive activity all locate to the HK module and, surprisingly, these constitutive AgrC mutants respond differently to the non-cognate inhibitor of the wild-type (WT) receptor, AIP-II (Geisinger et al., 2009).

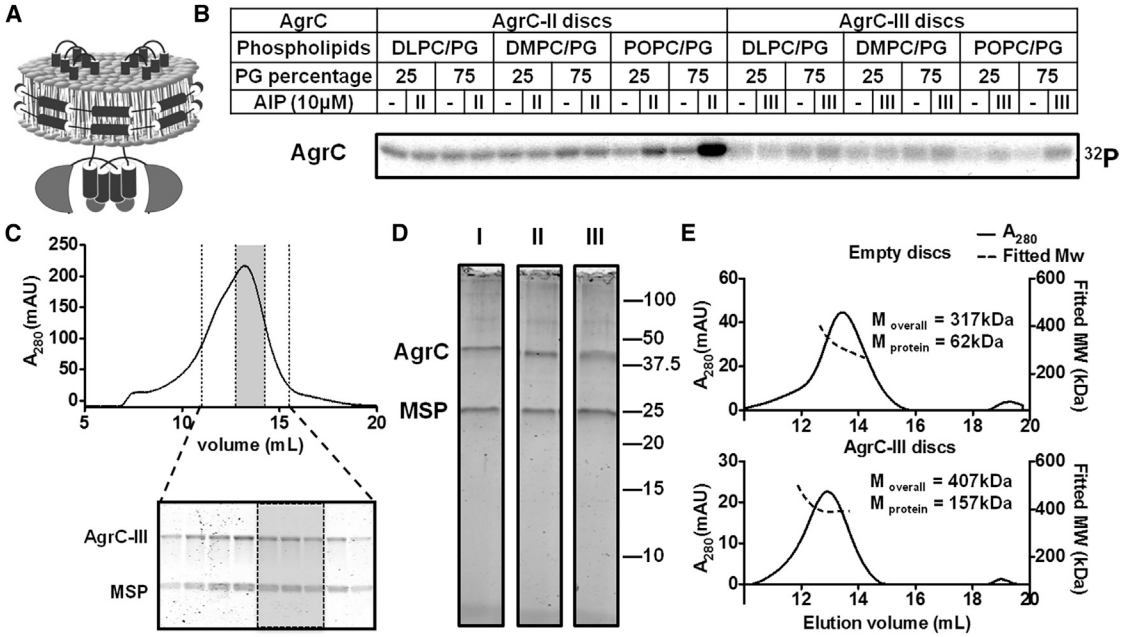

Figure 2. Functional Reconstitution of AgrC Homologs into Nanodiscs

(A) Cartoon of AgrC embedded in a nanodisc highlighting the open topology of the reconstituted system.

(B) Lipid-composition screen for the activation of AgrC-II and AgrC-III: 3 μM AgrC dimer, 12 μM MSP, and the appropriate amount of the indicated phospholipid stock were mixed and subject to detergent removal. The post-assembly mixtures, without further purification, were treated with 20 μM [γ-^{32}P]ATP, 10 mM $MgCl_2$, and 10 μM activator AIP (if indicated) at 37°C for 40 min. Phosphorylation levels were analyzed by autoradiography.

(C) SEC trace of Ni-NTA-purified AgrC-III nanodiscs: fractions between the dashed lines were further analyzed by SDS-PAGE with Coomassie brilliant blue (CBB) staining (inset). Shadow indicates the segment of elution collected as the product for further use. Lanes 5, 6, and 7 in the SDS-PAGE correspond to the gray area in the curve.

(D) Reconstitution of AgrC-I, -II, and –III into nanodiscs: 10 pmol of each nanodisc sample was resolved on SDS-PAGE and protein bands were visualized with CBB staining.

(E) SEC-MALS analysis of empty nanodiscs and purified AgrC-III discs. $M_{overall}$ corresponds to the experimental weight-average molecular weight (M_W) and $M_{protein}$ the M_W of protein content in each case. Note that each nanodisc contains two copies of MSP and each AgrC disc also contains one copy of AgrC dimer. Calculated molecular weight for monomers: AgrC-III = 52 kDa, MSP = 29 kDa.

A mechanistic understanding of the dysregulation of these mutants has yet to be established.

We have previously reconstituted full-length AgrC into nanometer-scale lipid-bilayer discs (nanodiscs) (Wang et al., 2014). This model membrane consists of a discoidal piece of lipid bilayer stabilized by an amphipathic-helical scaffold protein (Ritchie et al., 2009). The open topology of the bilayer enables simultaneous access of both intra- and extracellular domains of the receptor from the bulk solution (Figure 2A), thus allowing quantitative biochemical analyses at defined signaling states. In this study, we applied a similar strategy to full-length AgrC variants and mutants allowing for their detailed characterization and extended our investigations into the input-response relationship of their HK modules. We observed a striking correlation between the biochemical activities of AgrC variants in vitro and the temporal order of QS induction of their respective *agr* subgroups in cells. Two constitutive mutations, R238H and R238K, were found to dramatically modulate the input-response relationship of the HK module and, consequently, influence the activity of the full-length receptor in terms of baseline activity and ligand response. Collectively, these findings reveal considerable plasticity in AgrC signaling behavior when subject to sequence perturbations occurring in either its sensor or HK module.

RESULTS

Functional Reconstitution of Three AgrC Variants in a Uniform Lipid Composition

We chose AgrC-I, -II, and –III for a comparative analysis. Note, AgrC-IV was omitted from this study since it is closely related to AgrC-I both in sequence (it is activated by both AIP-IV and AIP-I) and in autoinduction timing in cells (Geisinger et al., 2012; Jarraud et al., 2000). The three homologs were successfully expressed in *Escherichia coli* (Figure S2A) and, following isolation, their identities and purity were verified by MALDI-TOF mass spectrometry (Figure S2B). We have previously reported the reconstitution of fully functional (i.e., AIP-dependent activity) AgrC-I embedded in nanodiscs containing 1,2-dimyristoyl-sn-glycero-phosphocholine (DMPC) and 1,2-dimyristoyl-sn-glycero-phosphoglycerol (DMPG) at a molar ratio of 1:3 (Wang et al., 2014). Importantly, a lipid bilayer enriched in anionic lipids (e.g., DMPG) is required for AgrC-I activation upon AIP-I binding, likely because it mimics the electrostatic environment of the native *S. aureus* membrane (Beining et al., 1975). Unexpectedly, AgrC-II and AgrC-III experience only slight activation by their cognate AIPs when embedded in discs comprising the same lipids (Figure 2A). In search of a membrane environment that

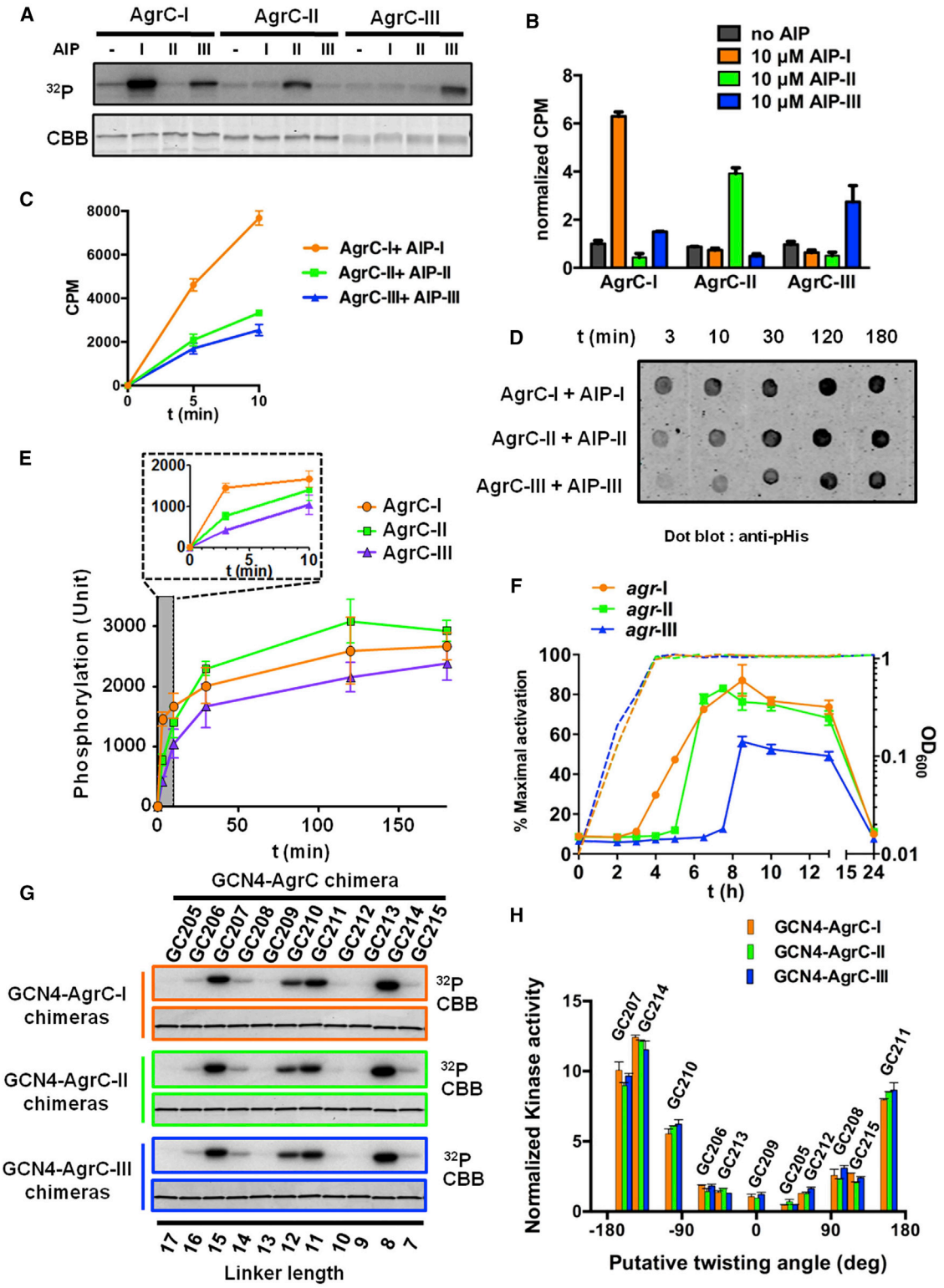

Figure 3. AIP-Dependent Autokinase Regulation of Full-Length AgrC Variants

(A and B) Autokinase analysis with AgrC variants and different AIPs: 0.7 μM AgrC-embedded nanodiscs were treated with indicated AIPs or vehicle and phosphorylated with 20 μM [γ-^{32}P]ATP at 37°C for 40 min. pHis levels were analyzed by autoradiography (A) or quantified using scintillation counting (B). A CBB-stained gel is used as a loading control. Note, AgrC-III consistently runs as a more diffuse band compared with the other variants. Densitometry analysis of the gel confirms equal loading (data not shown). The bar graph shows CPM values normalized to the average counts of AgrC-I without ligands. Error bars = SD (n = 3).

(legend continued on next page)

bolsters their activation, we varied the fatty-acyl tail groups of the phospholipids used in the reconstitution. Gratifyingly, a mixture of 1-palmitoyl-2-oleyl-sn-glycero-phosphocholine (POPC) and 1-palmitoyl-2-oleyl-sn-glycero-phosphoglycerol (POPG) at 1:3 molar ratio supports robust activation of both receptors (Figure 2B). We therefore reconstituted all three AgrC variants with this lipid composition (see Experimental Procedures for details). The crude post-assembly mixture was purified using Ni-NTA affinity chromatography, followed by Superose-6 size exclusion chromatography (SEC) (Figures 2C and 2D). Fractions corresponding to AgrC nanodiscs with the desired one-dimer-per-disk stoichiometry were pooled as the product (shaded fractions in Figure 2C), and the stoichiometry was confirmed using multi-angle light-scattering (MAL) experiments (Figure 2E).

We next tested the effect of AIP-I, -II, and -III on each reconstituted AgrC homolog (Figures 3A and 3B). As expected, AgrC-I was strongly activated by AIP-I and inhibited by AIP-II, similar to what had been observed with the DMPC-DMPG nanodiscs (Wang et al., 2014). Interestingly, a slight but significant activation was observed in the presence of AIP-III, while other combinations involving non-cognate AIP and AgrC pairs showed inhibitory effects, with AIP-II on AgrC-I the most significant (Figures 3A and 3B). Notably, AgrC-I exhibited the strongest activation level in the presence of excess cognate AIPs, followed by AgrC-II, then AgrC-III (Figures 3A–3C). Importantly, this difference is not due to a lower quality of reconstitution for AgrC-II or AgrC-III, as all three AgrC discs achieved roughly similar levels of endpoint phosphorylation after prolonged incubation with 1 mM ATP and the cognate AIPs (Figures 3D and 3E). Therefore, intrinsic kinetic variation exists among the activated states of these homologs. Intriguingly, the activity ranking of these AgrC homologs in their activated states is consistent with the temporal order of the QS induction timing of their respective subgroups (Geisinger et al., 2012). We experimentally confirmed that, on an isogenic background, the most active homolog, i.e., AgrC-I, leads to the earliest *agr* induction, while cells harboring the least active AgrC-III induce at highest densities (Figure 3F). Thus, the observed variation of autokinase activity, as revealed by our biochemical studies, likely plays a role in setting up the distinct QS schedule of individual *agr* allelic variants.

Activity of the HK Modules from AgrC Allelic Variants

Sequence variations among *S. aureus* AgrC subgroups predominantly localize to the sensor domain (see Figure S3). Indeed, the HK modules from the homologs have been thought to possess indistinguishable biochemical activities (Lyon et al., 2002a), despite mismatches at a handful of positions (Figure S4). To experimentally test this notion, we applied the aforementioned chimeric protein approach to all three HK-module variants. Our previous studies indicate that the linker region connecting the sensor and HK modules in AgrC (residues 201–221 in AgrC-I numbering) adopts an α-helical conformation and likely forms a contiguous helix with the N-terminal part of the DHp subdomain (Figure 1B) (Wang et al., 2014). Since the linker sequences are identical among the three AgrC variants, we fused a coiled-coil sequence from the leucine-zipper transcription factor, GCN4, to the N terminus of each residue in the linker region in a sequential fashion. This yielded a nested set of 11 GCN4-AgrC^{HK} (GC) chimeras for each HK module, i.e., 33 proteins in total (Figures 1C and 3G, Table S1) (Wang et al., 2014). The nomenclature used to describe these chimeras is based on the HK-module subgroup and the AgrC-residue number at the fusion junction. For instance, the chimera joining the GCN4 peptide to the AgrC-III fragment beginning at residue 205 is named GC205-III. Assuming that the GCN4 coiled coil acts as a rigid body in all chimeras and that the α helicity propagates from the GCN4 to the interdomain linker, the first residue of the AgrC fragment should be re-positioned to a uniform register in all chimera proteins (Figure 1D). In this regard, full-length AgrC-I at the resting state shares a similar linker conformation with GC209-I as was revealed by an inter-subunit crosslinking experiment (Wang et al., 2014). Using this as a reference, the magnitude by which the linkers are twisted away from the resting conformation can be estimated for all other chimeras based on the α-helical periodicity (Figure 1E).

The three series of chimeric proteins were produced and the autokinase activity of each quantified and plotted against the calculated twisting angle of the interdomain linker (Figures 3G and 3H). The resulting response curve reports on the intrinsic biochemical activity of each HK module. By this measure, the activity of the three HK modules is essentially identical, in spite of the sequence mismatches (Figure S4). Thus, the full-length AgrC variants exhibit different autokinase activity upon activation likely because their sensor modules adopt disparate conformations in the activator-bound state.

Modification of the Response Curve by Constitutive Mutations

Constitutively active versions of AgrC-I have been identified via screening of a random mutagenesis library for mutants that

(C) Autokinase reactions of AgrC variants with cognate AIPs at 5 and 10 min. Phosphorylation levels were quantified with scintillation counting, Error bars = SD (n = 3).
(D and E) Saturable autokinase time courses for AgrC variants: 0.7 μM AgrC-embedded nanodiscs were treated at 37°C with 1 mM ATP and 10 μM activator AIP (note the higher concentration of ATP used in this experiment compared with that in A, B, and C). Equal aliquots were removed at indicated time points and analyzed on a dot blot (D). AgrC phosphorylation detected by anti-pHis immunoblotting was quantified and plotted versus reaction time (E). In (E), inset shows a zoom-in for early time points. Error bars = SD (n = 3).
(F) In vivo kinetics of autoinduction mediated by *agr* allelic variants: *S. aureus* cells engineered to carry a chromosome-integrated *agr* allele were grown in a rich medium. Colored lines show the β-lactamase activity expressed from an AgrA-dependent reporter gene as a function of time. Activity values were normalized to the maximum activation, i.e., the highest value in the assay. Dashed lines are growth curves of subject strains. Error bars = SD (n = 3).
(G and H) Autokinase activities of GCN4-AgrC-I/II/III chimeras: dimeric chimeras (1.4 μM) were treated with 20 μM [γ-^{32}P]ATP at 37°C for 40 min. Phosphorylation of all three sets of proteins was visualized on the same autoradiogram (G) and quantified employing densitometry (H). The autokinase activity was then normalized to an internal standard of full-length AgrC-I without ligands (not shown) and plotted against the putative twisting angles to profile the response curve of each HK-module variant. In (G), linker length (in residues) between the GCN4 coiled coil and the HK module is indicated for each chimera construct. In (H), to avoid overlap, the dataset for GCN4-AgrC-I (orange bars) and GCN4-AgrC-III (purple bars) chimera series were shifted by 5° along the horizontal axis to the left and right, respectively. Error bars = range (n = 2).

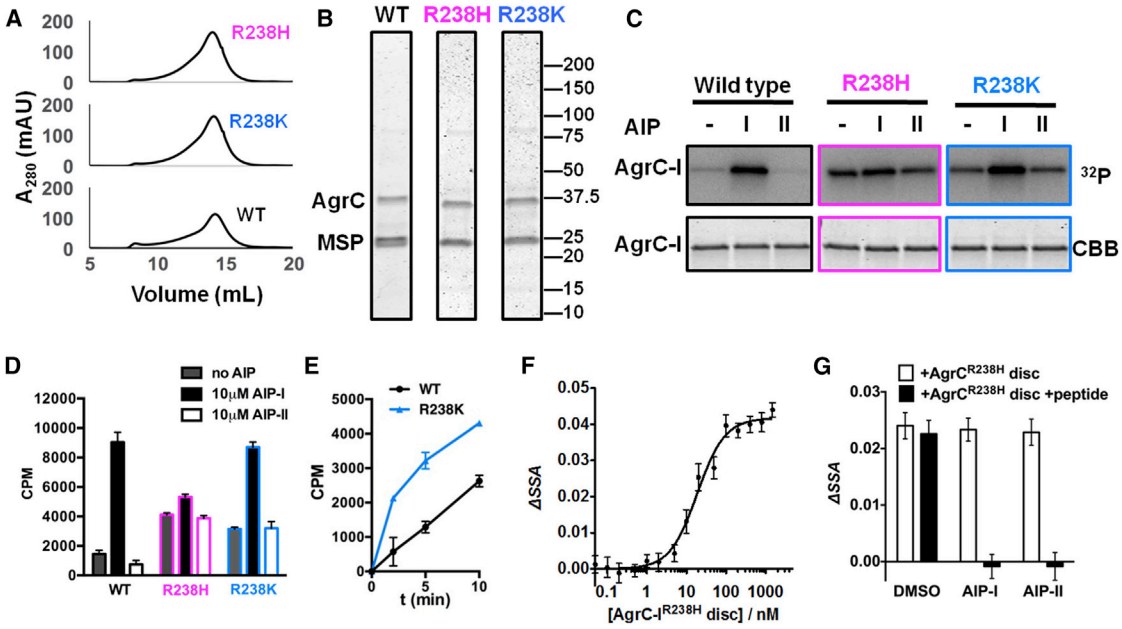

Figure 4. Reconstitution of AgrC-I Constitutive Mutants into Nanodiscs

(A) SEC traces of Ni-NTA-purified post-assembly nanodiscs containing R238H (top), R238K (middle), or WT (bottom) AgrC-I.

(B) As in Figure 2D, SDS-PAGE analysis of the nanodisc products containing WT and mutant AgrC-I variants.

(C and D) Autokinase activities of AgrC-I constitutive mutants visualized with autoradiography (C) or quantified with scintillation counting (D). Assays were performed following the procedures described in Figures 3A and 3B. Error bars = range (n = 2).

(E) Time course of autophosphorylation reactions on AIP-I bound AgrC-I^{WT} (black) and AgrC-I^{R238K} (blue). Reactions were assembled in the same way as in (C) and (D), and equal aliquots were removed at 2, 5, and 10 min. Autophosphorylation was quantified with scintillation counting. Error bars = range (n = 2).

(F) Equilibrium binding of FAM-AIP-I to nanodiscs containing AgrC-I^{R238H} dimers. Increase of steady-state anisotropy of the FAM-AIP-I fluorescence (ΔSSA) as a consequence of added AgrC-I^{R238H} disc was plotted as a function of nanodisc concentration and fit to a Hill equation. One representative titration of three is shown. Error bars (technical) show SEM (n = 6).

(G) Competitive displacement of FAM-AIP-I by AIP-I or AIP-II from AgrC-I^{R238H} nanodiscs: 150 nM AgrC-I nanodiscs were treated with 20 nM of FAM-AIP-I. SSA changes relative to free FAM-AIP-I were measured before and after addition of the indicated AIP (10 μM). Error bars = SD (n = 3).

activate AgrA-dependent reporter gene expression in the absence of AIP-I (Geisinger et al., 2009). A majority of such mutations occur in the HK module, with Arg238 (which is adjacent to the phospho-accepting His239) being the most common hotspot. Intriguingly, while AIP-II, the inverse agonist of the WT receptor, effectively represses the constitutive phenotype conferred by an Arg238Lys mutation, substitution of the same position with a Cys, Glu, Gly, or His results in a constitutive phenotype that is insensitive to AIP-II (Geisinger et al., 2009). To explore the mechanism(s) underlying this variance, we reconstituted AgrC-I^{R238H} and AgrC-I^{R238K} into nanodiscs for direct biochemical characterization. We again used POPC and POPG at a molar ratio of 1:3 for this reconstitution. Neither mutation had an effect on the solution behavior of the nanodiscs (Figures 4A and 4B). As expected from the in vivo phenotypes, both mutants are stronger autokinases than the WT receptor in the absence of ligands (Figures 4C and 4D). Despite having similar baseline activities, the two mutants responded differently to AIP-I; AgrC-I^{R238K} was activated 2- to 3-fold, whereas AgrC-I^{R238H} exhibited only marginal activation (Figures 4C, 4D, and S5). Moreover, autophosphorylation of AgrC-I^{R238K} was significantly faster than the WT in the presence of AIP-I (Figure 4E). Notably, AIP-II exercised limited inhibition on both constitutive mutants (Figures 4C and 4D). This insensitivity is in line with the cellular behavior of AgrC-I^{R238H} but inconsistent with that of AgrC-I^{R238K} where addition of AIP-II led to a decrease in *agr* activity (Geisinger et al., 2009). The latter discrepancy suggests that cellular inhibition of AgrC-I^{R238K} constitutive activity by AIP-II may not have occurred at the autokinase level (see below).

The muted responsiveness to AgrC-I^{R238H} to both AIPs motivated us to test whether it can bind these peptide ligands. Employing a fluorescent anisotropy-based approach (Johnson et al., 2015; Wang et al., 2014), we found that a fluorescein-tagged AIP-I (FAM-AIP-I) binds AgrC-I^{R238H} about twice as strongly as the WT (51 nM versus 122 nM, Figure 4F) (Wang et al., 2014). Both AIP-I and AIP-II, when present at the working concentration in the autokinase assays (10 μM), completely displace FAM-AIP-I from the mutant receptor (Figure 4G). The AIP ligands are therefore expected to saturate the binding sites on the mutant receptor under our assay conditions.

Since Arg-238 is remote from the sensor module of AgrC, the conformational input that the mutant HK modules receive in each ligand state should be identical to WT AgrC-I. Hence, the distinct response to AIP ligands in the constitutive mutants presumably comes from altered input-response relationships. To test this idea, we determined response curves for HK modules bearing R238H or R238K mutations, again harnessing the chimeric protein strategy (Figures 5A and 5B, Table S1). In line with the

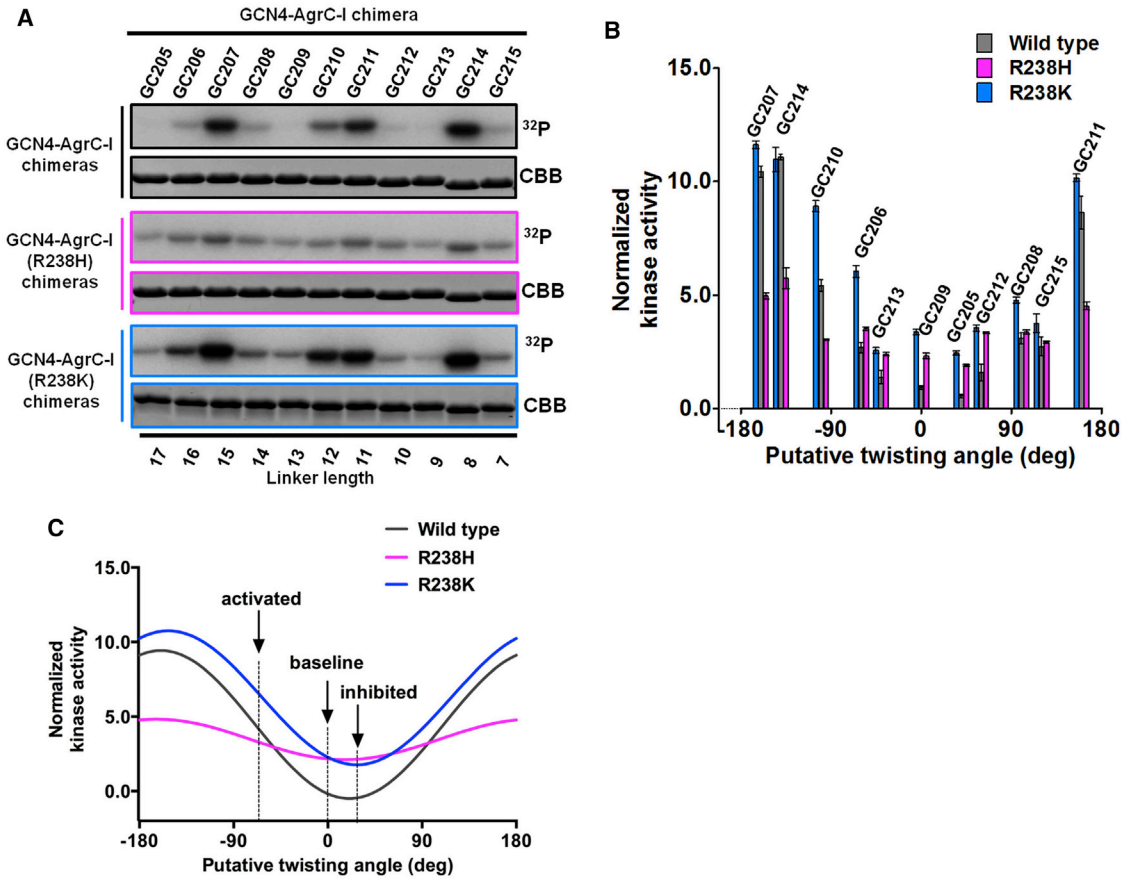

Figure 5. Input-Response Properties of the AgrC-I HK Modules Bearing the R238H or R238K Mutation

(A) Analogous to the data presented in Figure 4, autokinase activities of GCN4-AgrC-I chimeras containing the WT or mutant (R238H or R238K) HK modules were analyzed with autoradiography.

(B) The data in (A) were quantified by densitometry, normalized to an AgrC-I full-length internal control (not shown) and plotted against the calculated twisting angles to profile the response curves of the mutant HK modules. The dataset for GCN4-AgrC-I^{R238K} (blue bars) and GCN4-AgrC-I^{R238H} (pink bars) chimera series were shifted horizontally by 5° to avoid overlap. Error bars = SD (n = 3).

(C) Sinoidal fit of data in (B). Arrows and dashed lines mark the estimated twisting angle (determined previously; Wang et al., 2014) of full-length AgrC-I in the apo (baseline), AIP-I bound (activated), and AIP-II bound (inhibited) states.

behavior of the WT, the activity of both mutant HK modules responds gradually to the twisting motions of interdomain linkers. The phase of the response curves are also roughly unchanged compared with WT. This can be clearly seen by fitting each dataset to a sine function (Figure 5C). By contrast, both mutations perturb the activity maximum and minimum of the response curve. The R238H HK module, for instance, exhibited an increased activity minimum and a decreased maximum, with the amplitude of activity change dampened to about 30% of that of the WT, indicating lower sensitivity of the activity in respond to twisting force generated from different ligand binding states (Figures 5B and 5C). The higher baseline activity explains the constitutive activity of the full-length AgrC-I^{R238H} without AIP binding, and the lower activated activity and higher inhibited activity are consistent with the limited effect of AIP binding. The R238K mutation, by contrast, upshifted the entire response curve along the horizontal (activity) axis, in congruence with the consistently higher activity of AgrC-I^{R238K} relative to the WT receptor in all the baseline, activated, or inhibited states. This shows that a single mutation can affect the sensitivity of a sensor kinase to signal inputs, or generate an equal affect in all signaling states.

Mechanistic Understanding of AIP-II-Dependent Repression of AgrC-I^{R238K}

In contrast to its limited impact on the in vitro autokinase activity of AgrC-I^{R238K}, AIP-II effectively reverts the constitutive *agr*-active phenotype conferred by this mutation in vivo (Geisinger et al., 2009). Unlike most known RHKs, AgrC-I lacks detectable phosphatase activity (Wang et al., 2014). Therefore, the cellular repression is not likely a consequence of an induction of phosphatase activity by the binding of AIP-II. How then could AIP-II accomplish the repression observed in cells? To address this puzzle, we turned our focus to the phospho-transfer step between AgrC-I and AgrA. This step is often overlooked for its regulatory implications because it is not rate determining in the phospho-transfer cascade. To evaluate the ability of AgrC to produce phosphorylated AgrA (denoted as AgrA~P) under

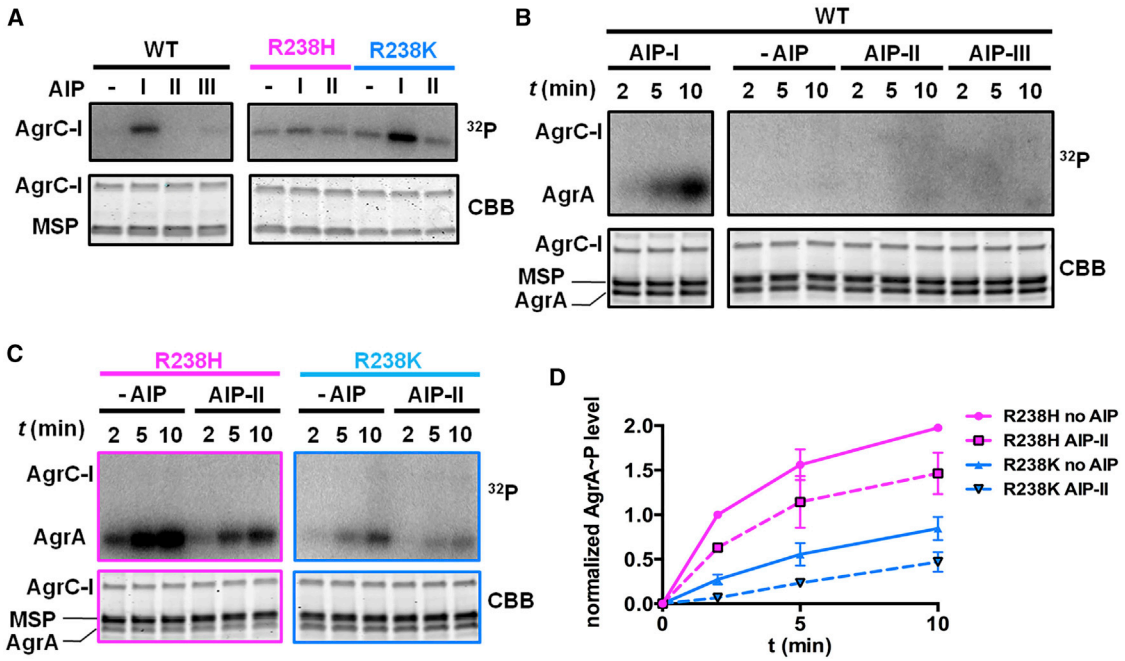

Figure 6. Behavior of WT and Mutant AgrC-I Variants in a Phospho-Transfer System

(A) Autokinase activities at elevated ATP concentration: 0.7 μM nanodiscs containing WT or indicated mutant AgrC-I were pre-incubated with 10 μM AIP (or vehicle) as indicated and treated with 500 μM [γ-^{32}P]ATP, 10 mM $MgCl_2$ at 37°C for 2 min. Phosphorylation was visualized using autoradiography.

(B and C) Production of AgrA∼P via phospho-transfer: 0.5 μM nanodiscs containing WT (B) or mutant AgrC-I (C) were incubated with 4 μM AgrA-I, 10 μM indicated AIP, and then treated with 500 μM [γ-^{32}P]ATP and 10 mM $MgCl_2$ at 37°C. Aliquots removed at indicated time points were resolved by SDS-PAGE and subject to autoradiography.

(D) Densitometry of (C) normalized to the average AgrA band density of R238H with no AIP at 2 min. Error bars = range (n = 2).

physiologically relevant conditions, we reconstituted the entire phospho-transfer cascade in a system that includes the nanodisc embedded RHK and an excess amount of the RR. The working concentration of ATP employed was 500 μM, i.e., on the same order as the K_m of AgrC-I (Wang et al., 2014), instead of the 20 μM typically used in our autokinase assays. This elevated ATP level should allow activated AgrC-I to phosphorylate an excess amount of AgrA through multiple phospho-transfer turnovers and therefore simulate the RHK's physiological behavior during *agr* induction (Wang et al., 2014). Importantly, the effect of AIPs and/or constitutive mutations on the autokinase activity of AgrC-I was unchanged at this elevated ATP concentration (compare Figures 6A with 4C).

The radiolabeled phosphoryl group was found exclusively on AgrA in all phospho-transfer reactions performed, i.e., there was no detectable phosphorylation on AgrC (Figures 6B–6D). The accumulation of AgrA∼P, as well as the efficacy of AIPs thereon, is remarkably consistent with findings made previously employing whole-cell-based assays (Geisinger et al., 2009; Lyon et al., 2002b). For instance, WT AgrC-I did not afford detectable levels of AgrA∼P unless activated by AIP-I (Figure 6B). Likely as a consequence, group I strains in the absence of AIP or in the presence of AIP-II or –III exhibit a uniform QS-off phenotype (Wright et al., 2005). Importantly, the inhibitory effect of AIP-II on the constitutive mutants became much more significant in the context of the phospho-transfer system (Figures 6C and 6D). In either ligand-free or AIP-II-bound states, AgrC-I^{R238H} produced AgrA∼P more efficiently than AgrC-I^{R238K} (Figures 6C and 6D), even though these mutants share almost indistinguishable autokinase activities in the absence of AgrA (Figures 4C and 6A). This finding sheds light on the AIP-II-insensitive and -revertible phenotypes conferred by AgrC-I^{R238H} and AgrC-I^{R238K}, respectively. AIP-II treatment likely reduces AgrA∼P levels in cells expressing either mutant, but to a level sufficient to downregulate AgrA-dependent transcription only in cells harboring AgrC-I^{R238K}.

DISCUSSION

The success of an organism relies on the exquisite adaptation of its sensory systems to stimuli that commonly exist in its habitat (Capra and Laub, 2012). At the molecular level, this adaptation often involves precise adjustment of the biochemical activities of signal-transduction proteins. This study showcases such biochemical tuning among *S. aureus* AgrC variants, which experience different magnitudes of autokinase activation when bound to their respective cognate AIP ligand. Remarkably, the activity ranking among these variants correlates with the temporal features of QS induction they mediate. We propose that the correlation results from the positive feedback loop that exists between AIP sensing and production in *agr* quorum sensing (Figure S1). With higher AgrC autokinase activity in the cognate AIP bound state, the TCS amplifies the signal to a larger extent in response to AIP binding, and so a lower AIP threshold level would be required to turn on the positive feedback in AIP production, ultimately leading to an earlier onset of quorum sensing in an *S. aureus* culture. Since the QS-induced gene products are

primarily involved in bacterium-host interactions (Novick and Geisinger, 2008), we speculate that the diverse stress conditions that the bacterium encounters during infection might contribute to the driving force for differentiation of the AgrCA TCS and the *agr* locus.

How do sequence variations among *S. aureus* AgrC homologs affect the autokinase activity of the RHK? Our finding that the HK modules of the variants possess indistinguishable input-response curves points to the sensor domain, where indeed the majority of sequence differences are found, as being the source of the observed activity differences. We therefore propose that distinct conformational inputs result from binding of cognate AIPs to the sensor domains of each AgrC subgroup. Testing this idea will require additional biochemical study, perhaps involving crosslinking approaches (Matamouros et al., 2015; Molnar et al., 2014; Saita et al., 2015; Wang et al., 2014), although high-resolution structural information on the system will ultimately be needed to fully understand these inputs.

In contrast to the behavior of intra-species variants of AgrC, two constitutive mutations, namely R238H and R238K, dramatically changed the input-response relationship of the HK module. Importantly, both mutations allow the HKs to exhibit significant baseline autokinase activity even when adopting conformations that would inactivate the WT HK (i.e., twisting angle around 0°, Figure 5C). Notably, the autokinase activity of an HK module is dictated by the conformational state of the DHp subdomain (Marina et al., 2005; Mechaly et al., 2014; Wang et al., 2013). Our results, therefore, imply that the conformations accessible to a DHp, as well as its responsiveness to external conformational inputs, are sensitive to particular mutations. In other words, variation of the input-response relationship can be achieved through surveying the local sequence space in an HK module. While the activity of *S. aureus* AgrC subgroups is not tuned by this mechanism, it is conceivable that this solution to molecular adaptation might play a role in the emergence of other closely related TCSs.

In our efforts to understand the dissimilar AIP-II-responses in *S. aureus* cells harboring the R238H and R238K mutants, we revealed, employing a reconstituted phospho-transfer assay, that the rate of AgrA∼P accumulation need not be proportional to the intrinsic autokinase activity of the mutant receptor. Thus, while the two constitutively active mutants have indistinguishable autokinase activities in the basal state, AgrC-I^{R238H} produced AgrA∼P much more efficiently than AgrC-I^{R238K}. As AgrC lacks detectable phosphatase activity (Wang et al., 2014), differences in the efficiency of the phospho-transfer step would seem to be the most likely explanation for this effect. Indeed, given the close proximity of residue 238 to the phospho-donor residue (i.e., His-239), it seems likely that this position is critical for the docking of AgrA on the HK domain of AgrC and that, by extension, mutations in this hotspot would alter the turnover rate of the phospho-transfer. More detailed biochemical and biophysical studies are necessary to test these ideas.

In conclusion, we have studied the biochemical consequences of the intra-species variation among *S. aureus* AgrC homologs and the mechanism underlying the constitutive activity of two AgrC-I mutants. Our efforts also provide insights that help reconcile the in vitro behaviors of the mutants with their responses to the AIP-II in vivo. We show that the conformational input from the sensor and the response curve of the HK can both be perturbed by sequence variation. The observed functional plasticity in AgrC underscores the potential of the RHKs for adaptive evolution in response to new environmental cues.

SIGNIFICANCE

AgrC is a receptor histidine kinase involved in the *agr* quorum sensing-circuit in *Staphylococcus aureus*, regulating biofilm formation and virulence factor secretion. Thus, it is viewed as a promising therapeutic target for *S. aureus* virulence inhibition. Characterization and mechanistic studies of AgrC may lay the groundwork for new treatments for *S. aureus* infection. We found that the rate of autokinase activity of the AgrCs in response to stimulation by their cognate AIP agonists is not the same. The rank order correlates with the order of QS induction. Thus, we provide a clear mechanistic explanation to account for the temporal differences in QS induction. We also examined two constitutive mutants of AgrC-I harboring single-point mutations in the HK domain (R238H and R238K). Remarkably, we see that these mutants also have different responses to AIPs both at the level of autokinase activity and phosphoryl-transfer activity to AgrA. The mechanism underlying the constitutive activity was revealed, namely that these single amino acid mutations can have profound impact on the response of the HK domain to a conformational input from the sensor. Thus, we have unearthed a key regulatory hotspot on the receptor histidine kinase. The observed functional plasticity in AgrC underscores the potential of the RHKs for adaptive evolution in response to new environmental cues.

EXPERIMENTAL PROCEDURES

Recombinant Proteins

Preparation of recombinant proteins relied on the pET system (Novagen) as previously reported (Wang et al., 2014). Briefly, coding sequences of all membrane-bound AgrC proteins were cloned between NdeI and XhoI sites of the pET24b plasmid and expressed in *E. coli* C43(DE3) cells. The total membrane fraction was isolated from cell lysates and extracted with Fos-choline-12. The membrane extract was subject to Ni-NTA affinity chromatography. Coding sequences of GCN4-AgrC chimeras were cloned into the pET15b plasmid using the same set of restriction sites and expressed in *E. coli* BL21(DE3) cells. Upon standard Ni-NTA affinity purification, the target protein was treated with thrombin to remove the hexahistidine tag. All proteins were further purified over Superdex 200 SEC before being used for reconstitution or biochemical assays. All purified GCN4-AgrC chimeras were characterized by electrospray ionization mass spectrometry. Mass spectrometry for full-length AgrC-I, AgrC-II, and AgrC-III was performed on a Spiral TOF JMS-S3000 (JEOL) MALDI-TOF instrument equipped with an Nd:YLF laser, following protocols described by Fenyo et al. (2007). Delayed extraction time was set at 1 μs and acquisition was performed with a sampling rate of 2 ns. Each MALDI spectrum acquired corresponded to an average of 1,500–2,000 scans. External calibration was performed with equine apomyoglobin. The spectra were processed and analyzed using MoverZ (Proteometrics).

Nanodisc Reconstitution of AgrC Variants

Nanodiscs were assembled following the general considerations described previously (Ritchie et al., 2009) and adapted to AgrC (Wang et al., 2014). Stocks of phospholipids (50 mM) were prepared in PBST buffer (20 mM phosphate [pH 7.5], 100 mM NaCl, 5 mM tris(2-carboxyethyl)phosphine [TCEP]) containing 150 mM sodium cholate. Lipids were mixed at the desired ratio prior

to the reconstitution. In the pre-assembly mixture, the stoichiometry between AgrC dimer and the membrane scaffold protein (MSP) was 1:4, aiming at two nanodiscs being formed for each AgrC dimer. Dimeric AgrC, MSP, and lipids were mixed at a molar ratio of 1:4:400 (1-palmitoyl-2-oleyl-sn-glycero (PO)-phospholipids), 1:4:500 (1,2-dimyristoyl-sn-glycerol (DM)-phospholipids) or 1:4:620 (1,2-dilauroyl-sn-glycerol (DL)-phospholipids). To set up the assembly mixture, MSP was incubated with the lipid stock and AgrC with 0.2% (w/v) Fos-choline-12, each for 20 min. Then, both mixtures were combined for another 20 min incubation before the addition of Bio-Beads SM2 (Bio-Rad, 25–30 mg for the removal of each milligram of sodium cholate) to remove detergents from the system. Upon incubation with Bio-Beads for 1.5 hr, the supernatant was withdrawn and subject to Ni-NTA purification. All incubation steps were carried out at 23°C for reconstitutions with PO and DL phospholipids and 30°C for those with DM lipids. Nanodiscs containing AgrC in the Ni-NTA eluate were further purified over a Superose-6 SEC column. SEC-MALS analysis of the nanodisc particle size and stoichiometry was carried out following established procedures (Wang et al., 2014, 2015).

Autokinase Assays

Autokinase reactions were performed as previously described with minor adjustments (Wang et al., 2014). A typical reaction included AgrC nanodisc or GCN4-AgrC chimera, AIP, and ATP at designated concentrations in a buffer system containing 50 mM Tris-HCl, 15 mM HEPES-Na (pH 7.8), 100 mM NaCl, 10 mM $MgCl_2$, and 1 mM TCEP. Reactions were incubated at 37°C for the indicated amount of time. Qualitative analysis of AgrC activity was carried out using autoradiography, where aliquots from the reaction containing 1–10 μCi [γ-^{32}P]ATP were mixed with loading dye and the mixture was resolved by SDS-PAGE. The gel was incubated with Eastman Kodak BIOMAX MR film. Quantitative analysis of AgrC activity was achieved employing scintillation counting or immunoblotting with a pan-specific antibody recognizing phosphohistidine (pHis) (Kee et al., 2013). For these purposes, equal aliquots of the reaction mixture were taken at specified time points and the reaction was stopped either by freezing on dry ice or direct spotting on a nitrocellulose membrane. The AgrC autophosphorylation level was detected following previously established protocols (Wang et al., 2014). Notably, previous studies showed that deposition of AgrC nanodiscs to the nitrocellulose surface confers instant termination of the autokinase reaction (Wang et al., 2014). For all assays, control reactions lacking the AgrC nanodiscs were performed in parallel and used to background correct AgrC autophosphorylation levels.

Phospho-Transfer Assays

A typical phospho-transfer reaction was carried out as follows: 8 μL of AgrA stock (20 μM in 20 mM HEPES [pH 7.0], 100 mM NaCl, 2 mM TCEP, and 15% (v/v) glycerol), 4 μL of buffer (20 mM HEPES-Na [pH 7.0], 100 mM NaCl, and 100 mM $MgCl_2$), 4 μL of AIP stock (100 μM in 27% [v/v] DMSO [or the vehicle]) and 4 μL of [γ-^{32}P]ATP (5 mM, 1.8 μCi/μL in 50 mM HEPES-Na [pH 7.0]) were mixed thoroughly and left on ice. To start the reaction, 20 μL of 1 μM AgrC nanodiscs was quickly mixed in and the reaction was immediately moved to a 37°C water bath. At each time point, 12 μL of the reaction was withdrawn, mixed with loading dye, and left frozen on dry ice to prevent hydrolysis of the labile AgrA~P. All samples were then thawed and immediately resolved on SDS-PAGE for visualization by autoradiography.

Fluorescent Polarization-Based Analysis of the AIP-AgrC Interaction

Measurement of the binding affinity between FAM-AIP-I and AgrC-I^{R238H} and the competitive displacement of FAM-AIP-I from AgrC-I^{R238H} by native AIP-I and AIP-II were carried out following procedures described previously (Johnson et al., 2015; Wang et al., 2014).

β-Lactamase Assay

Autoinduction was detected using a β-lactamase reporter as previously reported (Geisinger et al., 2012). Congenic strains EG802, EG803, and EG804 harboring *agr-I*, *-II*, or *-III* allele respectively, were employed in this study. Briefly, cells were grown overnight, spun down, and resuspended in fresh media. The starting OD_{600} was 0.01. Supernatants of cell cultures containing secreted AIPs were collected at the indicated time points and added to reporter strains expressing cognate AgrC-A promoted β-lactamase. The β-lactamase activity was assayed using nitrocefin as a substrate.

SUPPLEMENTAL INFORMATION

Supplemental Information includes five figures and one table and can be found with this article online at http://dx.doi.org/10.1016/j.chembiol.2016.12.008.

AUTHOR CONTRIBUTIONS

B.W., A.Z., and T.W.M. designed the research. B.W. and A.Z. developed and prepared recombinant protein and nanodisc reagents. B.W., A.Z., and Q.X. performed biochemical assays. P.D.O. and B.T.C. performed MALDI-TOF characterization of full-length AgrC proteins. B.W., A.Z., Q.X., R.P.N., and T.W.M. analyzed the data. B.W., A.Z., and T.W.M. wrote the manuscript.

ACKNOWLEDGMENTS

The authors would like to acknowledge members of the Muir Group for valuable discussions. This work was supported by NIH grants AI042783, GM095880, and GM103314 (B.T.C.).

Received: June 28, 2016
Revised: October 21, 2016
Accepted: December 13, 2016
Published: January 5, 2017

REFERENCES

Beining, P.R., Huff, E., Prescott, B., and Theodore, T.S. (1975). Characterization of lipids of mesosomal vesicles and plasma-membranes from *Staphylococcus aureus*. J. Bacteriol. *121*, 137–143.

Bhate, M.P., Molnar, K.S., Goulian, M., and DeGrado, W.F. (2015). Signal transduction in histidine kinases: insights from new structures. Structure *23*, 981–994.

Capra, E.J., and Laub, M.T. (2012). Evolution of two-component signal transduction systems. Annu. Rev. Microbiol. *66*, 325–347.

Casino, P., Rubio, V., and Marina, A. (2010). The mechanism of signal transduction by two-component systems. Curr. Opin. Struct. Biol. *20*, 763–771.

Fenyo, D., Wang, Q., DeGrasse, J.A., Padovan, J.C., Cadene, M., and Chait, B.T. (2007). MALDI sample preparation: the ultra thin layer method. J. Vis. Exp. *192*, http://dx.doi.org/10.3791/192.

Gao, R., and Stock, A.M. (2009). Biological insights from structures of two-component proteins. Annu. Rev. Microbiol. *63*, 133–154.

Geisinger, E., Muir, T.W., and Novick, R.P. (2009). Agr receptor mutants reveal distinct modes of inhibition by staphylococcal autoinducing peptides. Proc. Natl. Acad. Sci. USA *106*, 1216–1221.

Geisinger, E., Chen, J., and Novick, R.P. (2012). Allele-dependent differences in quorum-sensing dynamics result in variant expression of virulence genes in *Staphylococcus aureus*. J. Bacteriol. *194*, 2854–2864.

Jarraud, S., Lyon, G.J., Figueiredo, A.M.S., Gerard, L., Vandenesch, F., Etienne, J., Muir, T.W., and Novick, R.P. (2000). Exfoliatin-producing strains define a fourth agr specificity group in *Staphylococcus aureus*. J. Bacteriol. *182*, 6517–6522.

Ji, G.Y., Beavis, R., and Novick, R.P. (1997). Bacterial interference caused by autoinducing peptide variants. Science *276*, 2027–2030.

Johnson, J.G., Wang, B.Y., Debelouchina, G.T., Novick, R.P., and Muir, T.W. (2015). Increasing AIP macrocycle size reveals key features of agr activation in *Staphylococcus aureus*. Chembiochem *16*, 1093–1100.

Kee, J.M., Oslund, R.C., Perlman, D.H., and Muir, T.W. (2013). A pan-specific antibody for direct detection of protein histidine phosphorylation. Nat. Chem. Biol. *9*, 416–421.

Koenig, R.L., Ray, J.L., Maleki, S.J., Smeltzer, M.S., and Hurlburt, B.K. (2004). *Staphylococcus aureus* AgrA binding to the RNAIII-agr regulatory region. J. Bacteriol. *186*, 7549–7555.

Krell, T., Lacal, J., Busch, A., Silva-Jimenez, H., Guazzaroni, M.E., and Ramos, J.L. (2010). Bacterial sensor kinases: diversity in the recognition of environmental signals. Annu. Rev. Microbiol. *64*, 539–559.

Lyon, G.J., Wright, J.S., Christopoulos, A., Novick, R.P., and Muir, T.W. (2002a). Reversible and specific extracellular antagonism of receptor-histidine kinase signaling. J. Biol. Chem. *277*, 6247–6253.

Lyon, G.J., Wright, J.S., Muir, T.W., and Novick, R.P. (2002b). Key determinants of receptor activation in the agr autoinducing peptides of *Staphylococcus aureus*. Biochemistry *41*, 10095–10104.

Marina, A., Waldburger, C.D., and Hendrickson, W.A. (2005). Structure of the entire cytoplasmic portion of a sensor histidine-kinase protein. EMBO J. *24*, 4247–4259.

Matamouros, S., Hager, K.R., and Miller, S.I. (2015). HAMP domain rotation and tilting movements associated with signal transduction in the PhoQ sensor kinase. MBio *6*, e00616-15.

Mechaly, A.E., Sassoon, N., Betton, J.M., and Alzari, P.M. (2014). Segmental helical motions and dynamical asymmetry modulate histidine kinase autophosphorylation. PLoS Biol. *12*, e1001776.

Moglich, A., Ayers, R.A., and Moffat, K. (2009). Design and signaling mechanism of light-regulated histidine kinases. J. Mol. Biol. *385*, 1433–1444.

Molnar, K.S., Bonomi, M., Pellarin, R., Clinthorne, G.D., Gonzalez, G., Goldberg, S.D., Goulian, M., Sali, A., and DeGrado, W.F. (2014). Cys-scanning disulfide cross linking and bayesian modeling probe the transmembrane signaling mechanism of the histidine kinase, PhoQ. Structure *22*, 1239–1251.

Novick, R.P., and Geisinger, E. (2008). Quorum sensing in staphylococci. Annu. Rev. Genet. *42*, 541–564.

Qiu, R.D., Pei, W.H., Zhang, L.S., Lin, J.Q., and Ji, G.Y. (2005). Identification of the putative staphylococcal AgrB catalytic residues involving the proteolytic cleavage of AgrD to generate autoinducing peptide. J. Biol. Chem. *280*, 16695–16704.

Ritchie, T.K., Grinkova, Y.V., Bayburt, T.H., Denisov, I.G., Zolnerciks, J.K., Atkins, W.M., and Sligar, S.G. (2009). Reconstitution of membrane proteins in phospholipid bilayer nanodiscs. Methods Enzymol. *464*, 211–231.

Saita, E., Abriata, L.A., Tsai, Y.T., Trajtenberg, F., Lemmin, T., Buschiazzo, A., Dal Peraro, M., de Mendoza, D., and Albanesi, D. (2015). A coiled coil switch mediates cold sensing by the thermosensory protein DesK. Mol. Microbiol. *98*, 258–271.

Wang, B., and Muir, T.W. (2016). Regulation of virulence in *Staphylococcus aureus*: molecular mechanisms and remaining puzzles. Cell Chem. Biol. *23*, 214–224.

Wang, C., Sang, J.Y., Wang, J.W., Su, M.Y., Downey, J.S., Wu, Q.G., Wang, S.D., Cai, Y.F., Xu, X.Z., Wu, J., et al. (2013). Mechanistic insights revealed by the crystal structure of a histidine kinase with signal transducer and sensor domains. PLoS Biol. *11*, e1001493.

Wang, B.Y., Zhao, A.S., Novick, R.P., and Muir, T.W. (2014). Activation and inhibition of the receptor histidine kinase AgrC occurs through opposite helical transduction motions. Mol. Cell *53*, 929–940.

Wang, B., Zhao, A., Novick, R.P., and Muir, T.W. (2015). Key driving forces in the biosynthesis of autoinducing peptides required for staphylococcal virulence. Proc. Natl. Acad. Sci. USA *112*, 10679–10684.

Wright, J.S., 3rd, Traber, K.E., Corrigan, R., Benson, S.A., Musser, J.M., and Novick, R.P. (2005). The agr radiation: an early event in the evolution of staphylococci. J. Bacteriol. *187*, 5585–5594.